J Biomol NMR (2015) 61:89–94
DOI 10.1007/s10858-014-9888-1

COMMUNICATION

$^{13}C_{\alpha}$ CEST experiment on uniformly ^{13}C-labeled proteins

Yang Zhou · Daiwen Yang

Received: 10 October 2014 / Accepted: 26 November 2014 / Published online: 4 December 2014

Abstract A new HSQC-based $^{13}C_{\alpha}$ CEST pulse scheme is proposed, which is suitable for uniformly ^{13}C- or ^{13}C, ^{15}N-labeled samples in either water or heavy water. Except for Thr and Ser residues, the sensitivity of this scheme for uniformly labeled samples is similar to that of the previous scheme for selectively $^{13}C_{\alpha}$-labeled samples with 100 % isotope enrichment. The experiment is demonstrated on an acyl carrier protein domain. Our $^{13}C_{\alpha}$ CEST data reveal that the minor state of the acyl carrier protein has high helical propensity. The new scheme will facilitate structural characterization of invisible minor states.

Keywords Chemical exchange saturation transfer · Conformational exchange · Excited state · Protein dynamics

Chemical exchange saturation transfer (CEST) has emerged as a powerful technique for characterizing protein minor conformations which are in relatively slow exchange with the major conformation (Fawzi et al. 2011; Bouvignies and Kay 2012; Vallurupalli et al. 2012; Vallurupalli and Kay 2013; Lim et al. 2014; Zhao et al. 2014). Similar to relaxation dispersion experiments (Korzhnev and Kay 2008; Loria et al. 2008), CEST experiments provide not only kinetics parameters but also chemical shifts of minor conformations. The number of minor conformations existing in an exchange system is often not evident directly from relaxation dispersion data obtained by CPMG (Mittermaier and Kay 2006; Long and Yang 2010; Lim et al. 2012) or $R_{1\rho}$ techniques (Palmer and Massi 2006) and is model-dependent, but it can be obvious from CEST data when the exchange rate between the minor and major conformations is not much larger than the resonant frequency difference of a spin in these two conformations (Vallurupalli et al. 2012; Lim et al. 2014). During the CEST period, magnetization is aligned along the longitudinal direction or Z-axis. Thus scalar J coupling does not interfere with CEST but interferes with CPMG. Nevertheless, the coupling may complicate CEST data analysis and reduce experimental sensitivity (Hansen et al. 2013; Vallurupalli and Kay 2013). So it is preferable to suppress the J coupling. For ^{15}N and ^{13}C CEST experiments, it is easy to suppress heteronuclear J couplings between $^{15}N/^{13}C$ and ^{1}H spins during the CEST period, but removal of the couplings between ^{15}N and ^{13}C spins and between ^{13}C spins is extremely difficult. In addition, suppression of homonuclear aliphatic ^{13}C couplings in the indirect ^{13}C dimension of a ^{13}C–^{1}H correlation spectrum is not easy unless a constant-time acquisition mode (Santoro and King 1992; Vuister and Bax 1992) is used, which always causes significant sensitivity loss. A straightforward solution is to use ^{15}N-labeled samples for ^{15}N CEST experiments and a selectively ^{13}C labeled (e.g., $^{13}C_{\alpha}$-labeled) sample for a particular ^{13}C CEST experiment. The existing $^{13}C_{\alpha}$ CEST experiment has been developed based on $^{13}C_{\alpha}$-labeled samples (Hansen et al. 2013). The disadvantages of this selective labeling approach include the use of multiple samples (which may differ slightly), higher cost and more time-consuming in sample preparation when more than one types of spin probes have to be utilized for characterizing invisible minor states.

Very recently, we have developed an approximation method to analyze CEST data of ^{13}C and ^{15}N spins that are

Electronic supplementary material The online version of this article (doi:10.1007/s10858-014-9888-1) contains supplementary material, which is available to authorized users.

Y. Zhou · D. Yang (✉)
Department of Biological Sciences, National University of Singapore, 14 Science Drive 4, Singapore 117543, Singapore
e-mail: dbsydw@nus.edu.sg

weakly coupled with their neighboring spins in uniformly ^{13}C, ^{15}N-labeled samples (Zhou and Yang 2014). With this method, the effect of J couplings on the extraction of kinetics parameters can be taken into account properly and consistent results have been obtained from ^{13}CO and ^{15}N CEST data using a single ^{13}C, ^{15}N-labeled sample. Since $^{13}C_\alpha$ chemical shift is a better reporter of protein backbone secondary structure than ^{13}CO and ^{15}N shifts, determination of $^{13}C_\alpha$ chemical shifts of minor states will be important for characterization of minor state structures. Here we present a new $^{13}C_\alpha$ CEST experiment on uniformly ^{13}C- or ^{13}C, ^{15}N-labeled samples.

Figure 1 shows the pulse scheme for recording $^{13}C_\alpha$ CEST data by using uniformly ^{13}C, ^{15}N-labeled protein samples. The pulse sequence is similar to the gradient-enhanced HSQC-type scheme (Kay et al. 1992), i.e., both N- and P-type coherence pathways are selected for sensitivity enhancement. In this sequence, the critical elements include $^{13}C_\alpha$–$^{13}C_\beta$ decoupling during the indirect ^{13}C dimension and water suppression for samples in 90–95 % water. In order to obtain high resolution and high sensitivity spectrum, undesired J couplings have to be suppressed. From point *a* to *b*, anti-phase $^{13}C_\alpha H_\alpha$ magnetization is refocused and its dephasing by $^{13}C_\alpha$–$^{13}C_\beta$ couplings is prevented using a selective $^{13}C_\alpha$ 180° pulse in the middle of the refocusing period. Similarly, a selective $^{13}C_\alpha$ 180° pulse is used in the middle of the period from point *g* to *h* to avoid the same type of magnetization dephasing. Longitudinal $^{13}C_\alpha$ magnetization is generated at point *b*. Subsequently, a purge pulse element is applied to suppress water signals just before the CEST. During the CEST period, $^{1}H_\alpha$–$^{13}C_\alpha$ couplings are removed by using a train of composite inversion pulses ($90_x240_y90_x$) as proposed by Kay's group (Vallurupalli et al. 2012). After the CEST, another purge pulse element is applied to further suppress the residual water signals. To minimize water signals, the lengths of the purge X and Y pulses are adjustable, which were in the range of 450–650 μs for our tested samples in a solution of 95 % water and 5 % heavy water.

From point *c* to *g*, the $^{13}C_\alpha$ magnetization is encoded with ^{13}C chemical shifts and as well is transferred back to $^{1}H_\alpha$ magnetization. The J couplings between $^{13}C_\alpha$ and ^{15}N spins and between $^{13}C_\alpha$ and ^{13}CO are removed by using a ^{15}N 180° pulse and a selective ^{13}CO 180° pulse at point *d*, respectively. Immediately after the ^{13}CO pulse, a selective $^{13}C_\beta$ 180° pulse is employed to suppress the couplings between $^{13}C_\alpha$ and $^{13}C_\beta$ spins. In order to effectively suppress ^{13}C–^{13}C couplings, the $^{13}C_\alpha$ 180° pulse at point *f* should not disturb $^{13}C_\beta$ and ^{13}CO spins. The $^{13}C_\beta$ and

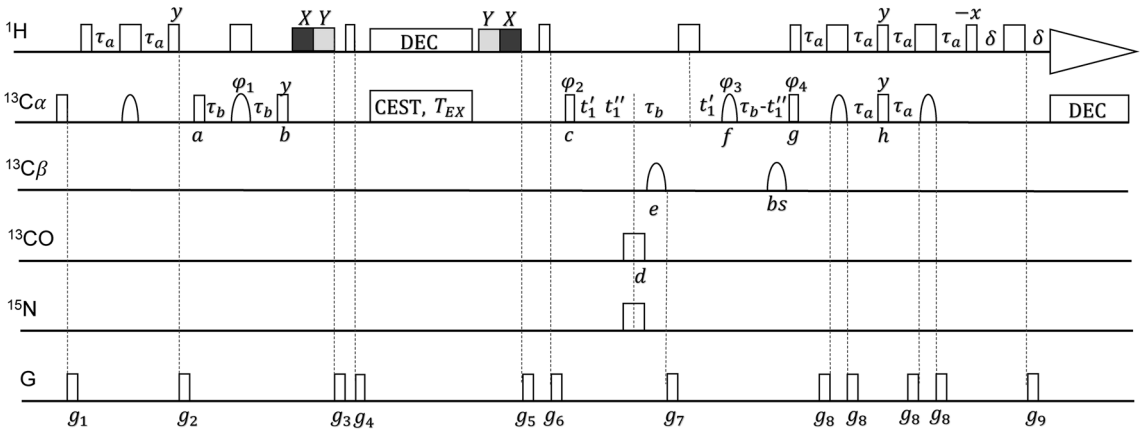

Fig. 1 Pulse scheme for $^{13}C_\alpha$ CEST experiments. All narrow (*wide*) rectangular pulses (*open*) are applied with a flip angle of 90° (180°). The carriers are centred at 4.7, 59.2 and 119 ppm for ^{1}H, ^{13}C and ^{15}N, respectively. The *grey* and *dark* ^{1}H pulses are applied with a field strength of 10 kHz and their respective durations are about 500 and 650 μs. The *shaped* $^{13}C_\alpha$ 180° pulses have a REBURP profile centred at 59.2 ppm. The $^{13}C_\alpha$ 180° pulse at point *f* has a duration of 1,000 μs, while others have a duration of 800 μs. The *shaped* $^{13}C_\beta$ 180° pulses have an IBURP profile (800 μs) centred at 30.9 ppm. The ^{13}CO 180° pulse is applied with a field strength of $\Delta/\sqrt{15}$, where Δ is the resonant frequency difference of $^{13}C_\alpha$ and ^{13}CO spins. A Bloch–Siegert compensation pulse is applied at the position indicated by '*bs*'. ^{1}H decoupling during the CEST period is achieved using repetition of $90_x240_y90_x$ composite pulse with a field strength of 2.272 kHz. $^{13}C_\alpha$ saturation is done with weak CW radiofrequency fields. Quadrature detection for t_1 dimension was achieved by the enhanced sensitivity pulse field gradient method (Kay et al. 1992). The gradients used were: G1 (*sine-shaped* 1 ms, 5 G/cm), G2 (*sine-shaped* 1 ms, 22.5 G/cm), G3 (*sine-shaped* 1.8 ms, 30 G/cm), G4 (*sine-shaped* 2 ms, 13.25 G/cm), G5 (*sine-shaped* 2 ms, 12.5 G/cm), G6 (*sine-shaped* 2 ms, 26.5 G/cm), G7 (*rectangular* 0.1 ms, −40 G/cm), G8 (*sine-shaped* 1 ms, 25 G/cm), and G9 (*rectangular* 0.1 ms, 10.05 G/cm). The delays used were: $\tau_a = 1.6$ ms, $\tau_b = 1.72$ ms and $\delta = 0.2$ ms. The increments for t_1'' and t_1' are $(\tau_b - pw_{C\beta})/(TD_1 - 1)$ and $0.5/SW_C - t_1''$, where $pw_{C\beta}$ is the length of the $^{13}C_\beta$ 180° pulse, TD_1 is the total complex points in the t_1 dimension and SW_C is the spectral width of the indirect ^{13}C dimension. The phase cycling used was: φ_1 = x, y, −x, −y; φ_2 = y, φ_3 = x, x, −x, −x, φ_4 = x, and φ_{rec} = x, −x

$^{13}C_\alpha$ chemical shifts for residues other than Gly, Ser and Thr are often in the ranges of 17–44 and 51–68 ppm, respectively (http://www.bmrb.wisc.edu/ref_info/statsel.htm#5, statistics calculated for selected chemical shifts from atoms in the common amino acids). Therefore, it is possible to suppress the $^{13}C_\alpha$–$^{13}C_\beta$ couplings in most residues by using a $^{13}C_\beta$ 180° pulse centered at 30.7 ppm with an inversion bandwidth of 26 ppm at point *e* and a $^{13}C_\alpha$ 180° pulse centered at 59.2 ppm with a refocusing bandwidth of 20 ppm at point *f*. For Ser and Thr residues, because their $^{13}C_\alpha$ and $^{13}C_\beta$ chemical shifts usually differ by less than 10 ppm, the $^{13}C_\alpha$–$^{13}C_\beta$ couplings are difficult to be removed. In this pulse scheme, thus the $^{13}C_\alpha$–$^{13}C_\beta$ couplings for Ser and Thr remain unsuppressed. In cases where $^{13}C_\beta$ chemical shifts are larger than 44 ppm, incomplete decoupling will be observed in the ^{13}C dimension, which may occur for some Leu residues.

For Gly residues, the C–H correlations are not observable when delay τ_b is set to $1/4J_{CH}$ since each $^{13}C_\alpha$ spin couples to two ^1H spins. In order to use one of the τ_b delays between points *c* and *g* for acquisition, a semi-constant-time acquisition mode in the indirect dimension is employed (Grzesiek and Bax 1993; Logan et al. 1993). In comparison with the constant-time experiment, the scheme used here is more sensitive and the sensitivity enhancement (S) is roughly given by

$$S = \frac{\int_0^{At} \exp(-R \times t)dt}{AT \times \exp(-R \times T)} = \frac{1 - \exp(-R \times AT)}{AT \times \exp(-R \times T)} \quad (1)$$

where R is the transverse relaxation rate of $^{13}C_\alpha$, T is the duration of the constant-time period and is normally set as 28 ms, and AT is the total acquisition time in the ^{13}C dimension in this scheme. When the data are acquired on an 800 MHz spectrometer and AT = T = 28 ms, S = 1.5 for a protein with an overall tumbling time of 7 ns (~100 residues at 25 °C). The larger the protein is, the larger the sensitivity enhancement will be. Compared with a selectively $^{13}C_\alpha$-labeled sample, a uniformly labeled sample will give rise to similar experimental sensitivity since undesired ^{13}C–^{13}C couplings are removed during the magnetization transfer and indirect acquisition periods, but will display broader CEST dips because the J couplings are not suppressed during the CEST period. Selective labeling at C_α position can be easily achieved using [2-^{13}C]-glucose for 17 types of amino acids, but Leu, Ile and Val that are key hydrophobic residues cannot be labeled in a selective manner (Lundström et al. 2007). In addition, the $^{13}C_\alpha$ enrichment level is always smaller than 50 %, namely the effective protein concentration is <50 % of the total protein concentration. Therefore, the experimental sensitivity of the scheme shown here for uniformly labeled samples can be significantly higher than the sensitivity of the previous scheme for samples selectively labeled with 2-^{13}C-glucose when the total sample concentrations are similar.

The pulse scheme proposed here was demonstrated on an acyl carrier protein from *Micromonospora echinospora* spp. *Calichensis* (*me*ACP). *me*ACP is a small protein domain (92 residues) with three helices connected by two long loops (Lim et al. 2011). Using ^{15}N CEST, we have recently shown that *me*ACP exists in three states under native conditions: one folded stated (95.2 %), one unfolded state (4.1 %) and one intermediate state (0.7 %). The three states undergo conformational exchanges with exchange rates less than 250 s^{-1} at 25 °C (Lim et al. 2014). Interestingly, the intermediate is an off-pathway rather than on-pathway folding product.

$^{13}C_\alpha$ CEST experiments were performed on an 800 MHz NMR spectrometer equipped with a cryoprobe and z-gradients using a uniformly ^{13}C, ^{15}N-labeled *me*ACP sample which was prepared by following previous protocols (Lim et al. 2011). The sample contained 0.6 mM labeled protein, 50 mM NaCl, 5 mM EDTA, 20 mM phosphate at pH 6.9, and 5 % D_2O. The NMR data were acquired with two weak RF fields of 17.6 and 35.2 Hz. For each RF field, 51 2D HSQC spectra were acquired with a series of ^{13}C carrier frequencies ranging from 50.2 to 70.2 ppm at an interval of 0.4 ppm. Each 2D data set comprised 640 × 100 complex points in the ^1H and ^{13}C dimensions and was recorded with 4 scans, an inter-scan delay of 1.5 s, a saturation time (T_{EX}) of 0.5 s, and spectral widths of 9,615 Hz for ^1H and 4,024 Hz for ^{13}C. A reference spectrum was also acquired using similar parameters except that $T_{EX} = 0.05$ s. The acquisition time in the ^{13}C dimension was 27.1 ms. The total experimental time was ~56 h.

Figure 2 shows the $^{13}C_\alpha$ CEST spectrum of *me*ACP in 95 % H_2O and 5 % D_2O recorded when the weak B_1 field was applied at 50.2 ppm. Except Thr and Ser which give rise to doublets due to $^{13}C_\alpha$–$^{13}C_\beta$ couplings, other residues display singlets and their $^{13}C_\alpha$–$^{13}C_\beta$ couplings are effectively suppressed. The noise from residual water signals is distributed in a very small region (about 0.2 ppm). For *me*ACP, no $^1H_\alpha$ is located in the noise region. When a cryoprobe equipped with x, y and z gradients or a room temperature probe is used, better water suppression can be achieved. The excellent water suppression and effective $^{13}C_\alpha$–$^{13}C_\beta$ decoupling for residues other than Thr and Ser allow characterizing slow motions with $^{13}C_\alpha$ spins using uniformly ^{13}C-labeled samples in H_2O.

Figure 3 shows typical $^{13}C_\alpha$ CEST profiles. Most residues in α1, α2, α3, loop1 and loop2 display two obvious dips, several residues in the N-terminal region of α2 display 3 dips, and all residues in the disordered N- and C-terminal regions display only one dip. The chemical shifts of the minor state were obtained from the CEST

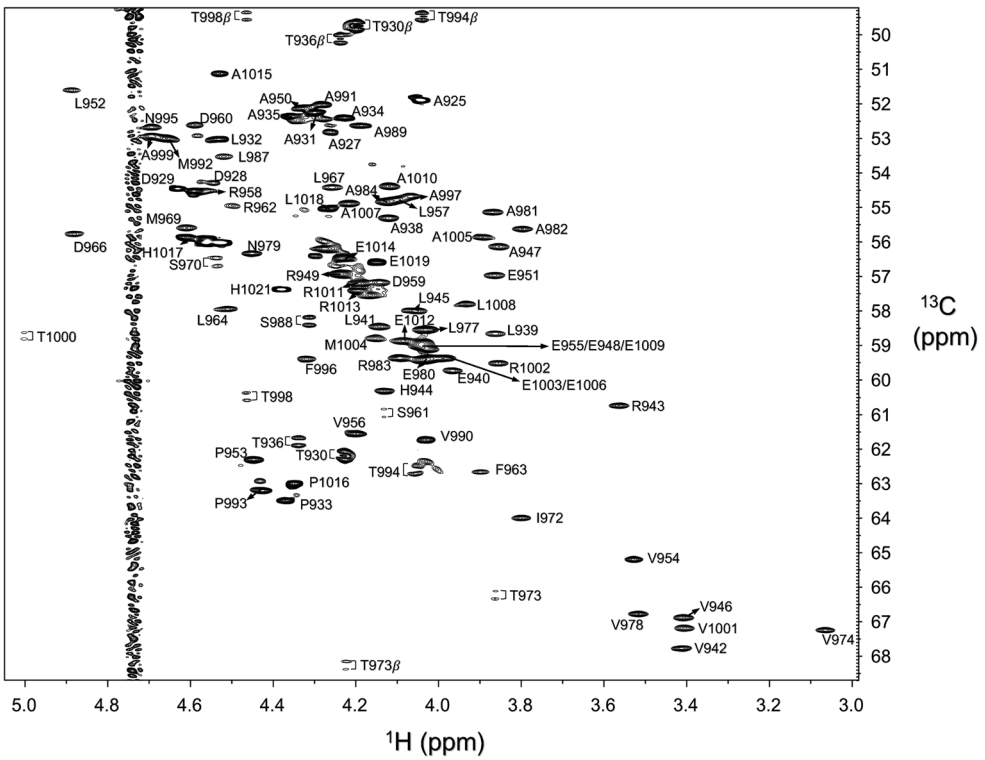

Fig. 2 $^{13}C_\alpha$ CEST ^{1}H–^{13}C correlation spectrum of *me*ACP in 95 % H_2O and 5 % D_2O. The noise in the region around 4.73 ppm is from residual water signals. The $^{1}H_\beta$–$^{13}C_\beta$ correlations located at around 50 ppm (from Thr) are aliased by 22 ppm

profiles with two obvious dips by using our J-coupling-considered method (Zhou and Yang 2014) and assuming $^{1}J_{C\alpha C\beta} = 35$ Hz and $^{1}J_{C\alpha CO} = 55$ Hz. The minor state displays significantly larger $^{13}C_\alpha$ chemical shifts than a random coil state (Fig. 4). The average differences are 0.6 ppm for helix 1 (α1: A938-R949), 0.8 ppm for helix 2 (α2: S971-M985), and 1.0 ppm for helix 3 (α3: V1001-R1013), which are much larger than the fitting errors (<0.05 ppm). However, they are significantly smaller than the average shift differences between the major state and random coil state (3.0 ppm for helix 1, 3.3 ppm for helix 2 and 2.6 ppm for helix 3). It is noteworthy that the method used to predict the chemical shifts of the random coil state has been shown to be robust (Tamiola et al. 2010). Therefore, the minor state is mainly unfolded, consistent with the conclusion drawn from our previous ^{15}N CEST and relaxation dispersion studies (Lim et al. 2012, 2014). Moreover, the data obtained here show that the minor state retains significant helical propensity in the original helical regions. Interestingly, the C-terminal region of loop 1 also possesses helical propensity (Fig. 4). In fact, the ^{15}N shifts of the minor state which were derived from ^{15}N CEST data are systematically smaller than those of the denatured state in 4 M urea (Fig. 1d in Lim et al. 2014), further supporting the presence of helical propensity of the minor state. Besides $^{13}C_\alpha$ shifts, the exchange rate between the minor and major state (304 s^{-1}) and the population of the minor state (4.0 %) were obtained from the $^{13}C_\alpha$ CEST data. The results are consistent with those derived from our previous ^{15}N (275 s^{-1} and 3.85 %) and ^{13}CO (293 s^{-1} and 3.6 %) CEST data (Zhou and Yang 2014) when the same ^{13}C, ^{15}N-labeled sample was used. On the other hand, they are significantly different from those obtained with a ^{15}N-labeled sample (218 s^{-1}, 4.7 %) (Lim et al. 2014). The difference may come from ^{13}C labelling or/and slight difference in sample buffers because the ^{15}N–^{1}H HSQC spectra of the two samples were slightly different, indicating the necessity of using a single sample for all the dynamics experiments.

The observation of three dips (Fig. 3c) demonstrates the presence of a second minor state, which is consistent with the conclusion drawn from our previous ^{15}N CEST data (Lim et al. 2014). Although T994 (located in the middle region of loop2) displays only one minor dip, the depth of the dip is much smaller than those for other residues with two dips (Fig. 3). This profile is caused by the overlap of the major dip with the first minor dip and the observed minor dip comes from the second minor state. Although S970 and T994 show doublets in the ^{1}H–$^{13}C_\alpha$ correlation spectrum (Fig. 2), the experimental sensitivity is good enough for extraction of their chemical shifts in the minor states. The $^{13}C_\alpha$ chemical shifts of S970 and T994 are 61.0 and 66.2 ppm in the second minor state, 58.9 and 62.8 ppm in the first minor state, and 56.6 and 62.8 ppm in the major state, indicating the second minor state adopts a distinct conformation from the major and first minor states.

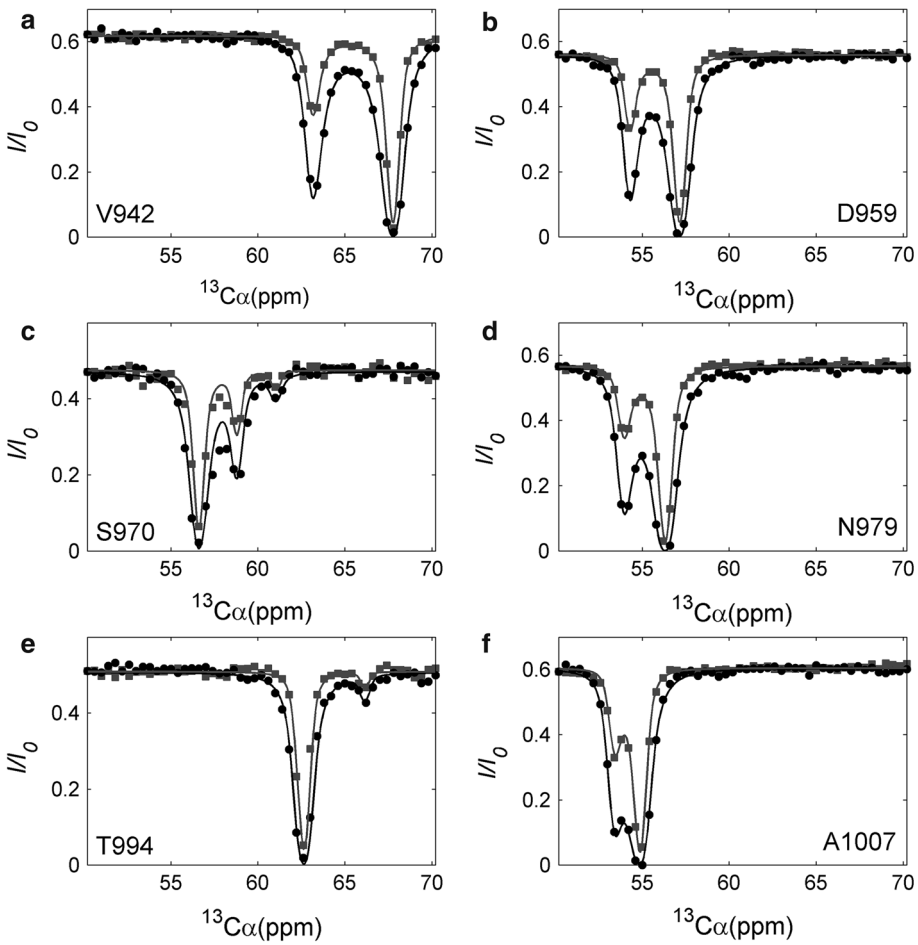

Fig. 3 Representative CEST profiles. The data points obtained at weak RF fields of 17.6 and 35.2 Hz are shown as *filled squares* and *circles*, respectively. The *solid curves* are the best fits with a two-state model (N ↔ U) or three state model (I ↔ N ↔ U)

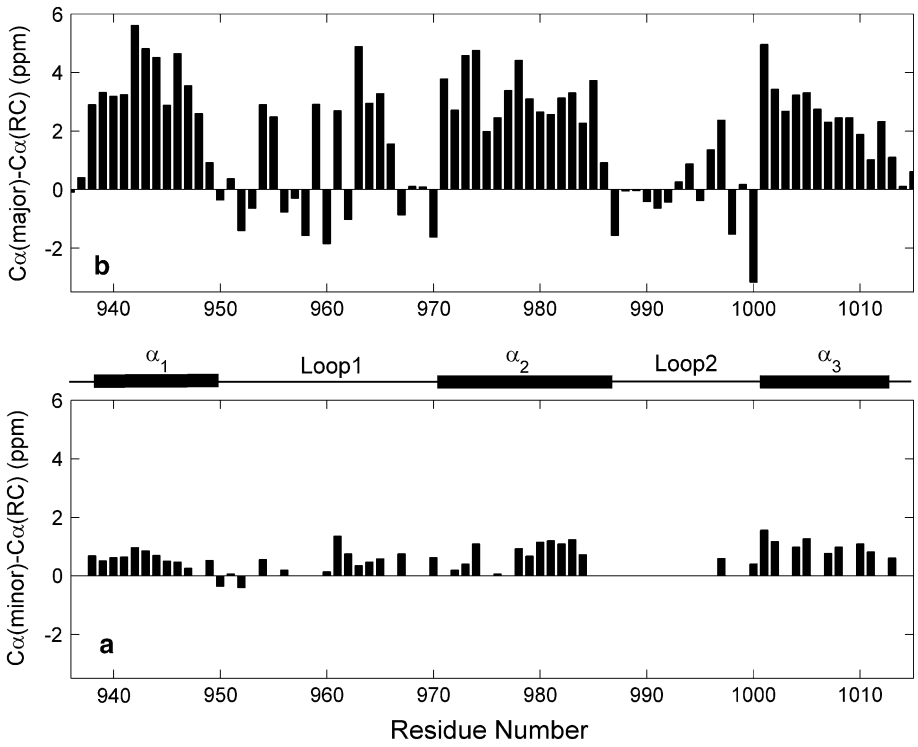

Fig. 4 $^{13}C_\alpha$ secondary chemical shifts for meACP in the minor state (**a**) and major state (**b**). The $^{13}C_\alpha$ chemical shifts of the minor state, C_α(minor), were derived from CEST data, while the shifts of the major state, C_α(major), were measured from the 2D HSQC shown in Fig. 2. The shifts of the random coil state, C_α(RC), were predicted using the online software by Tamiola et al. (http://nmr.chem.rug.nl/cgi-bin/start_session_FASTA.py). The secondary structure of the major state is shown schematically above panel **a**

In summary, the $^{13}C_{\alpha}$ CEST experiment proposed here supresses water signals very well and eliminates $J_{C\alpha C\beta}$ coupling effectively for 17 out of 19 amino acids. It is much more sensitive than triple resonance-based $^{13}C_{\alpha}$ CEST experiments. Moreover, the experimental sensitivity is independent of ^{13}C-labelling patterns and thus is very suitable for uniformly ^{13}C- or ^{13}C, ^{15}N-labeled samples. When multiple spin probes such as ^{15}N, ^{13}CO, $^{13}C_{\alpha}$ and $^{13}C_{\beta}$ are needed for structural characterization of minor states, the CEST experiments based on uniformly labelled proteins make it possible to use a single sample. Results obtained here further show that the first minor state of meACP is mainly unfolded but retains significant helical propensity.

Acknowledgments This work is supported by a Grant from Singapore Ministry of Education Academic Research Fund Tier 2 (MOE2012-T2-2-138).

References

Bouvignies G, Kay LE (2012) A 2d (1)(3)c-cest experiment for studying slowly exchanging protein systems using methyl probes: an application to protein folding. J Biomol NMR 53:303–310

Fawzi NL, Ying J, Ghirlando R, Torchia DA, Clore GM (2011) Atomic-resolution dynamics on the surface of amyloid-beta protofibrils probed by solution nmr. Nature 480:268–272

Grzesiek S, Bax A (1993) Amino acid type determination in the sequential assignment procedure of uniformly $^{13}C/^{15}N$-enriched proteins. J Biomol NMR 3:185–204

Hansen AL, Bouvignies G, Kay LE (2013) Probing slowly exchanging protein systems via 13Calpha-CEST: monitoring folding of the im7 protein. J Biomol NMR 55:279–289

Kay L, Paul Keifer P, Saarinen T (1992) Pure absorption gradient enhanced heteronuclear single quantum correlation spectroscopy with improved sensitivity. J Am Chem Soc 114:10663–10665

Korzhnev D, Kay L (2008) Probing invisible, low-populated states of protein molecules by relaxation dispersion nmr spectroscopy: an application to protein folding. Acc Chem Res 41:442–451

Lim J, Kong R, Murugan E, Ho CL, Liang Z-X, Yang D (2011) Solution structures of the acyl carrier protein domain from the highly reducing type I iterative polyketide synthase cale8. PLoS ONE 6:e20549

Lim J, Sun H, Fan J, Hameed I, Lescar J, Liang ZX, Yang D (2012) Rigidifying acyl carrier protein domain in iterative type i pks cale8 does not affect its function. Biophys J 103:1037–1044

Lim J, Xiao T, Fan J, Yang D (2014) An off-pathway folding intermediate of an acyl carrier protein domain coexists with the folded and unfolded states under native conditions. Angew Chem Int Ed Engl 126:2390–2393

Logan T, Olejniczak E, Xu R, Fesik S (1993) A general method for assigning nmr spectra of denatured proteins using 3D hc(co)nh-tocsy triple resonance experiments. J Biomol NMR 3:225–231

Long D, Yang D (2010) Millisecond timescale dynamics of human liver fatty acid binding protein: testing of its relevance to the ligand entry process. Biophys J 98:3054–3061

Loria JP, Berlow RB, Watt ED (2008) Characterization of enzyme motions by solution nmr relaxation dispersion. Acc Chem Res 41:214–221

Lundström P, Teilum K, Carstensen T, Bezsonova I, Wiesner S, Hansen D, Religa T, Akke M, Kay L (2007) Fractional 13C enrichment of isolated carbons using [1-^{13}C]- or [2-^{13}C]-glucose facilitates the accurate measurement of dynamics at backbone calpha and side-chain methyl positions in proteins. J Biomol NMR 38:199–212

Mittermaier A, Kay L (2006) New tools provide new insights in NMR studies of protein dynamics. Science 312:224–228

Palmer A, Massi F (2006) Characterization of the dynamics of biomacromolecules using rotating-frame spin relaxation NMR spectroscopy. Chem Rev 106:1700–1719

Santoro J, King G (1992) A constant-time 2d overbodenhausen experiment for inverse correlation of isotopically enriched species. J Magn Reson 97:202–207

Tamiola K, Acar B, Mulder F (2010) Sequence-specific random coil chemical shifts of intrinsically disordered proteins. J Am Chem Soc 132:18000–18003

Vallurupalli P, Kay LE (2013) Probing slow chemical exchange at carbonyl sites in proteins by chemical exchange saturation transfer nmr spectroscopy. Angew Chem Int Ed Engl 52:4156–4159

Vallurupalli P, Bouvignies G, Kay LE (2012) Studying "invisible" excited protein states in slow exchange with a major state conformation. J Am Chem Soc 134:8148–8161

Vuister G, Bax A (1992) Resolution enhancement and spectral editing of uniformly ^{13}C-enriched proteins by homonuclear broadband ^{13}C decoupling. J Magn Reson 98:428–435

Zhao B, Hansen AL, Zhang Q (2014) Characterizing slow chemical exchange in nucleic acids by carbon CEST and low spin-lock field R1ρ nmr spectroscopy. J Am Chem Soc 136:20–23

Zhou Y, Yang D (2014) Effects of J couplings and unobservable minor states on kinetics parameters extracted from CEST data. J Magn Reson 249:118–125